Research Article Vol. 2, No. 2 / February 2015 / Optica 95

Spatial coherence of sunlight and its implications for light management in photovoltaics

SHAWN DIVITT AND LUKAS NOVOTNY*

Photonics Laboratory, ETH Zürich, 8093 Zürich, Switzerland

**Corresponding author: lnovotny@ethz.ch*

Received 14 August 2014; revised 12 December 2014; accepted 12 December 2014 (Doc. ID 221013); published 27 January 2015

New technologies are emerging that capture and redirect sunlight inside solar cells. This type of light management can significantly increase efficiency, but the device behavior will fundamentally depend on the spatial coherence of the incoming light. This dependence calls for a complete characterization of the spatial coherence of sunlight. Here, we present the first spectral measurements of the spatial degree of coherence of direct, diffuse, and simulated sunlight. An expression is derived for both the cross-spectral density and the spatial degree of coherence in an arbitrarily oriented device plane, including the effects of overcast skies. Implications of the present work are discussed and may lead to a better understanding of light-managing components in solar cells as well as a new class of solar simulator that provides both the same spectrum and spatial coherence as direct sunlight.

OCIS codes: (030.1640) Coherence; (350.6050) Solar energy; (030.1670) Coherent optical effects.

http://dx.doi.org/10.1364/OPTICA.2.000095

1. INTRODUCTION

Multi-junction solar cells, which divide or selectively respond to portions of the solar spectrum, are the highest-efficiency cells ever produced [1]. However, spectral control is only a partial solution toward maximizing efficiency [2]; a complementary method for higher performance is the use of light-managing structures that capture or redirect light [3–12].

Light management can increase efficiency in single- and multi-junction cells, but the device behavior will depend on both the spatial coherence and the bandwidth of the incoming light [13]. The behavior of rectenna solar cells has similar dependencies [14,15]. It is therefore necessary to fully characterize the *spectral* variation of the *spatial* coherence of sunlight. We refer to devices whose behavior depends on spatial coherence as coherent photovoltaics or co-PVs.

The spatial coherence of direct terrestrial sunlight (sunshine) was first considered in the 19th century by Verdet [16]. Much more recently the machinery of modern coherence theory was applied to the calculation of the spectral degree of spatial coherence expected from sunshine by Agarwal *et al.* [17] and found to essentially match Verdet's expectation. Indeed, the mutual intensity of sunshine, a broadband quantity that is related to the spectral degree of coherence [18], was subsequently measured by Mashaal *et al.* [19] and found to substantially agree with the expectation [20]. However, the calculations of Agarwal *et al.* are based on a uniform sphere model and therefore ignore real optical effects such as solar limb darkening.

While the previous measurements demonstrate agreement with the theory in the broadband case, the spectral degree of coherence, which considers each spectral component separately, has not been measured. Further, if co-PVs are to be used in real applications, it is necessary to understand the spatial coherence of sunlight under non-ideal weather conditions as well as to establish a spatial coherence standard for device testing. Here, we present the first interferometric measurements of the transverse spectral degree of coherence of both direct sunshine and diffuse terrestrial sunlight, where the Sun is obscured by clouds or fog. In this context, transverse indicates that the coherence function is measured in a plane whose normal vector points directly toward the center of the Sun.

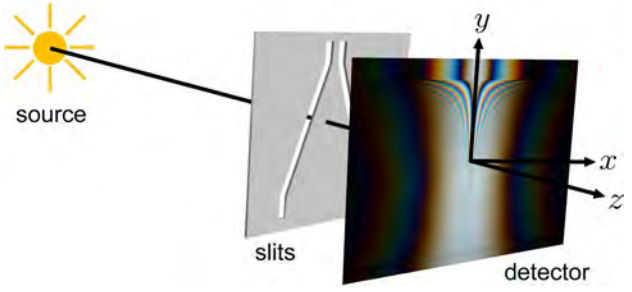

Fig. 1. Illustration of the experimental measurement procedure. Broadband light from the source passes through a pair of non-parallel slits creating an interference pattern on a detector.

Our measurements are performed using the method illustrated in Fig. 1. The method involves non-parallel slits and its working principles have been described previously [21]. The measurements are precise enough to distinguish between the expectations of uniform and limb-darkened incoherent spheres. To demonstrate the precision of the measurements, we compare our findings with those expected by theory as applied to hyperspectral solar limb darkening measurements made by Neckel and Labs [22]. We also present a measurement of the spectral degree of coherence of light emitted by a solar simulator, establishing the need for a spatial coherence standard in co-PV device testing.

To provide context to the measurements and their practical use, we present the theory of the spectral degree of coherence of sunlight beyond the transverse case and/or under a uniformly cloudy sky. Unless sophisticated tracking methods are used, a photovoltaic cell is generally never in a plane whose normal vector points directly toward the center of the Sun. Consequently, a description of how the coherence properties of sunlight vary with the position of the Sun in the sky relative to a fixed device plane is important to predict the behavior of co-PVs at different times in the day. We provide an expression that derives any non-transverse spectral degree of coherence function in terms of the measured transverse function. Having established these results, we discuss how to apply them to the simulation of co-PV devices.

2. PROBLEM STATEMENT

Spatial coherence is a measure for the correlation between optical fields in different locations of space. More specifically, we are interested in measuring the degree of spatial coherence, $\eta(\vec{r_1}, \vec{r_2}, \omega)$, which gives a scalar description of the statistical correlation between the fields with frequency ω at locations $\vec{r_1}$ and $\vec{r_2}$. In the following we will refer to $\eta(\vec{r_1}, \vec{r_2}, \omega)$ as the spectral degree of coherence [23]. In general, a degree of coherence can be described between any pair of field components for any pair of points in space. A rigorous description of second-order coherence is given by a 3×3 covariance matrix known as the cross-spectral density (CSD) matrix $\mathbf{W}(\vec{r_1}, \vec{r_2}, \omega)$ (see Mandel and Wolf [24], Sect. 6.6.1). The CSD matrix is directly applicable to the numerical simulation of light propagating in a solar cell (see Implications). However, the spectral degree of coherence can be more easily measured and provides evidence for the structure of a theoretical CSD matrix.

The spectral degree of coherence can be defined in terms of the CSD matrix as [23]

$$\eta(\vec{r_1}, \vec{r_2}, \omega) := \frac{\mathrm{Tr}[\mathbf{W}(\vec{r_1}, \vec{r_2}, \omega)]}{\sqrt{\mathrm{Tr}[\mathbf{W}(\vec{r_1}, \vec{r_1}, \omega)]}\sqrt{\mathrm{Tr}[\mathbf{W}(\vec{r_2}, \vec{r_2}, \omega)]}}, \quad (1)$$

where Tr denotes the matrix trace. The two-slit apparatus illustrated in Fig. 1 provides a simple and robust measurement of η as defined by Eq. (1) (see Appendix A). We note that alternative definitions of the spectral degree of coherence exist that take all elements of $\mathbf{W}$ into account [25]. However, the use of Eq. (1) is justified by the facts that direct and cloud-diffused sunlight are unpolarized [26] and therefore Eq. (1) represents the essential elements of $\mathbf{W}$. Partially polarized skylight (blue sky) is discussed as a separate case in Appendix E.

For scalar fields, the van Cittert-Zernike theorem has been traditionally used to calculate the CSD of sunshine (see Born and Wolf [27], Sect. 10.4.2). For electromagnetic fields, the general case can be calculated using an angular spectrum of plane waves propagating within a solid angle σ subtended by the source at the device plane. Under the assumption of angularly uncorrelated and unpolarized plane waves the CSD matrix is given by [28,29]

$$\begin{aligned}\mathbf{W}(\vec{r_1}, \vec{r_2}, \omega) &:= \langle \vec{E}^*(\vec{r_1}, \omega)\vec{E}^{\intercal}(\vec{r_2}, \omega)\rangle \\ &= \int_\sigma a(\hat{u}, \omega)(\mathbf{U}_3 - \hat{u}\hat{u}^{\intercal}) \exp(ik\hat{u}\cdot\vec{r})\mathrm{d}\Omega, \quad (2)\end{aligned}$$

where $\vec{E}$ is the random electric field column vector;

$$\hat{u} = -\sin\theta\cos\phi\hat{x} - \sin\theta\sin\phi\hat{y} - \cos\theta\hat{z}$$

is the unit vector that specifies the propagation direction of a plane wave (θ and ϕ represent polar and azimuthal spherical coordinates, respectively); the vectors $\hat{j}(j = x, y, z)$ are the unit column vectors along the coordinate axes (see Fig. 2(a)); $\mathrm{d}\Omega := \sin\theta\mathrm{d}\theta\mathrm{d}\phi$ is the differential solid angle; $k := \omega/c$ is the wavenumber; $\vec{r} := \vec{r_2} - \vec{r_1}$; $\mathbf{U}_3$ is the 3×3 identity matrix; $a(\hat{u}, \omega)$ is, up to a constant, the average power spectral density per unit solid angle of waves traveling with frequency ω in the $\hat{u}$ direction; $*$ indicates complex conjugate; $\intercal$ indicates vector transpose; and the angle brackets indicate an ensemble average over monochromatic field realizations. Equation (2) immediately implies, under the given assumptions, that $\mathbf{W}(\vec{r_1}, \vec{r_1}, \omega) = \mathbf{W}(\vec{r_2}, \vec{r_2}, \omega)$ and that $\mathbf{W}(\vec{r_1}, \vec{r_2}, \omega)$ is a function of $\vec{r}$ alone such that we can write $\mathbf{W}(\vec{r}, \omega)$ and $\eta(\vec{r}, \omega)$ in their respective places. For a very distant source, the function $a(\hat{u}, \omega)$ is given by the power spectral density distribution of the source that is apparent from the origin (see Novotny and Hecht [30], Sect. 3.4).

In general, the device plane shown in Fig. 2(a) can have an arbitrary orientation with respect to the source. We first consider the special case of a device plane that is transverse to a circularly symmetric source, that is, z in Fig. 2(a) passes through the center of the source. For this case we denote

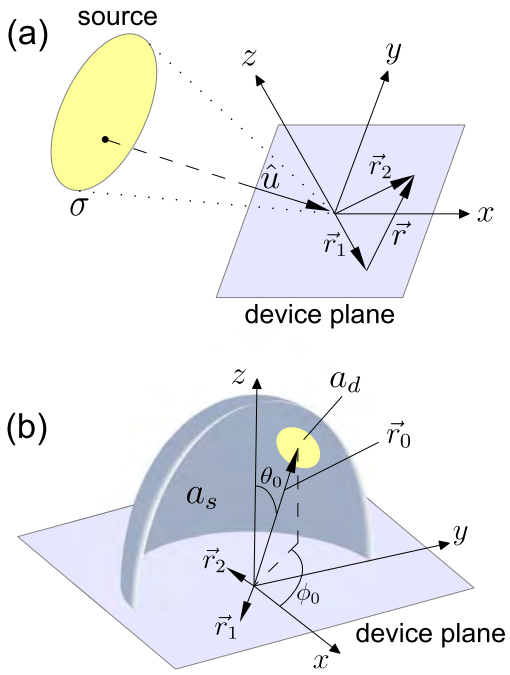

Fig. 2. Illustration of the theoretical model. (a) An plane wave propagating along the $\hat{u}$ direction is emitted from the corresponding position on a distant source σ. Positions $\vec{r}_1$ and $\vec{r}_2$ lie in the device (x, y) plane. (b) A cutaway illustration of a combined disk-shell source. The device plane is illuminated by diffuse light (half-shell source) with spectral density $a_s(\hat{u}, \omega)$ and by direct sunlight (disk source centered at $\vec{r}_0$) with spectral density $a_d(\hat{u}, \omega)$. The front portion of the half-shell has been removed to reveal the origin.

the spectral degree of coherence as $\eta_\perp$, or the *transverse* spectral degree of coherence. Due to rotational symmetry, $\eta_\perp(\vec{r}, \omega)$ is a function of $r := |\vec{r}|$ alone and can be written $\eta_\perp(r, \omega)$. Later, we will consider an arbitrarily oriented device plane and express η in terms of $\eta_\perp$ and orientational angles.

In the following we will distinguish between two different types of sources, direct sunshine and diffuse sunlight. The latter corresponds to a uniformly bright, cloudy sky. We model this situation with a spatially incoherent half-shell source whose radius is large, surrounding the device plane (see Fig. 2(b)). The origin of the device plane is placed at the center of the half-shell. The spectral degree of coherence in this case is given by (see Appendix B) [23,31]

$$\eta_s(\vec{r}, \omega) = \frac{\sin(k|\vec{r}|)}{k|\vec{r}|}. \tag{3}$$

This result indicates that, for a spatially incoherent half-shell source, the spatial coherence length along any direction at the center of the shell is on the order of one wavelength of the light.

Light illuminating the device plane is in general a mixture of direct and diffuse sunlight. We model this situation as the combination of a disk and a half-shell source, as shown in Fig. 2(b). Consequently, the spectral degree of coherence is given by (see Appendix C)

$$\eta(\vec{r}, \omega) = \frac{s_d}{s_d + s_s}\eta_d(\vec{r}, \omega) + \frac{s_s}{s_d + s_s}\eta_s(\vec{r}, \omega), \tag{4}$$

where s_d and s_s represent the spectral densities in the device plane due to the disk and shell, η_s is given by Eq. (3) and η_d is the spectral degree of coherence in the disk-only case as defined by Eqs. (1) and (2). Introducing the parameter $\gamma := s_d/(s_d + s_s)$, we can rewrite the equation above as

$$\eta(\vec{r}, \omega) = \gamma\eta_d(\vec{r}, \omega) + (1 - \gamma)\eta_s(\vec{r}, \omega). \tag{5}$$

In the next section we will use a simple experimental procedure to measure η in the transverse plane and compare the results with the theoretical model, Eq. (5).

3. EXPERIMENTAL RESULTS

We have fabricated a pair of non-parallel slits to measure the transverse spectral degree of coherence of i) direct sunshine, ii) light emitted by a solar simulator, and iii) diffuse sunlight (see Appendix A for materials and methods).

i) **Direct sunshine**: Figure 3 shows the measured and calculated transverse spectral degree of coherence $\eta_\perp(r, \omega)$ for direct sunshine with wavelength λ between points separated by a distance r. Both the amplitude and phase of $\eta_\perp$ are shown. The theoretical maps were calculated by applying Eqs. (1) and (2) to hyperspectral measurements of solar limb darkening [22] (see Appendix D). The excellent agreement of the two amplitudes is made clear by the cross sections, given in Fig. 4(a), along the lines indicated in Figs. 3(a) and 3(c) corresponding to a wavelength of 510 nm. For the phase we obtain similar good agreement (Fig. 4(b)), aside from inconsequential offsets of integer multiples of 2π.

We emphasize that the measured and calculated amplitudes do not strictly agree with previous theoretical estimates based

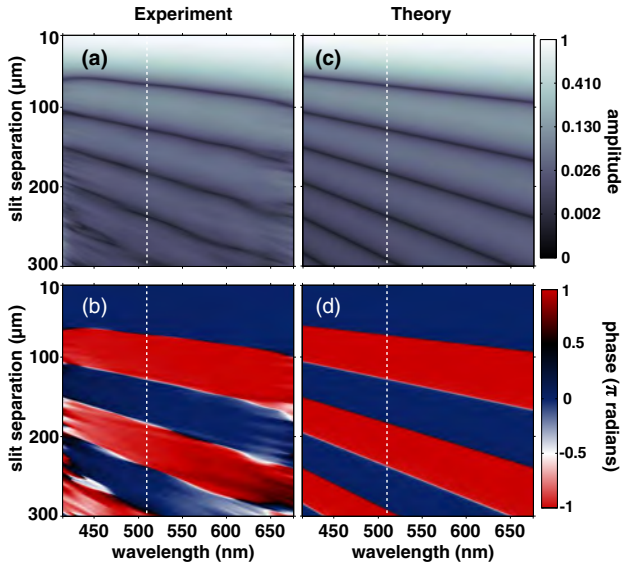

Fig. 3. Measured and calculated transverse spectral degrees of coherence $\eta_\perp$ of direct sunshine. Amplitude (a) and phase (b) of the transverse spectral degree of coherence measured by the double slit apparatus. Amplitude (c) and phase (d) of the spectral degree of coherence calculated by Eqs. (1) and (2) as applied to hyperspectral images of the Sun.

on the uniform incoherent sphere model [17]. The coherence amplitude function expected from a spatially uniform incoherent sphere source is shown in Fig. 4(a). The disagreement is minor; the estimate has an error of at most 10% for separations below 80λ and gets better for longer wavelengths. This result shows that solar limb darkening only weakly affects the coherence properties of sunlight at visible frequencies.

Our measurements of $\eta_\perp$ given in Fig. 3 can be used to derive a measure for the coherence length. For example, defining the coherence length $L_\perp$ as the slit separation for which the amplitude of $\eta_\perp$ decays to $1/2$, we find that $L_\perp = 80\lambda$ for direct sunshine.

ii) **Solar simulator**: The transverse spectral degree of coherence was also measured with a solar simulator source. Typically, such a simulator is used to test the performance of photovoltaic devices that are placed within a test area (device plane) where the power spectral density of the light approximately matches that of direct sunshine. It is evident that the measured $\eta_\perp$ of simulated sunlight, shown in Fig. 4(a), does not match the sunshine case. This serves to highlight the fact that the power spectral density at the device plane should not be the only consideration in solar simulator design. For solar cells whose performance depends on the coherence properties of light, a simulator should be used that renders both the correct power spectral density and the correct spatial coherence.

The requirements on such a simulator follow from Eq. (2): the source should not only have the same spectrum as the Sun but its size and shape should also be matched to render the same spatial coherence as sunshine. A hyperspectral set of images recorded from the point of view of the test area would appear identical to a hyperspectral set of images of the Sun, except perhaps for a global intensity scaling factor. As previously discussed, a uniform disk/sphere source approximates the spatial distribution of the Sun fairly well. Consequently, wavelength-dependent limb darkening can be safely dismissed in solar simulator design unless a very high degree of accuracy is required in measuring the device performance relative to that under direct sunshine.

iii) **Diffuse sunlight**: The measurements of diffuse sunlight are given in Fig. 5. In each case, the sky was completely and uniformly covered by clouds or fog in such a way that the position of the Sun was still discernible. Notably, the positions of the amplitude minima in the spectral degree of coherence remain unchanged under each measured weather condition while other aspects of the function change significantly. This fact is also borne out in the phase information as given in Fig. 4(b), where the steps in phase occur invariably at the same distances. Of interest is the behavior of the spectral degree of coherence relative to the direct sunshine case. From the inset in Fig. 5 it is noticeable that, in each diffuse case, the degree of coherence appears to be simply offset vertically from the direct sunshine case. This implies that the coherence functions in the diffuse cases can be described as fractions of the direct function, as implied by Eq. (5).

Indeed, the measurements in the diffuse case are well fitted by Eq. (5). The second term on the right-hand side of the equation falls off quickly and is negligible for $r > 5\lambda$, where

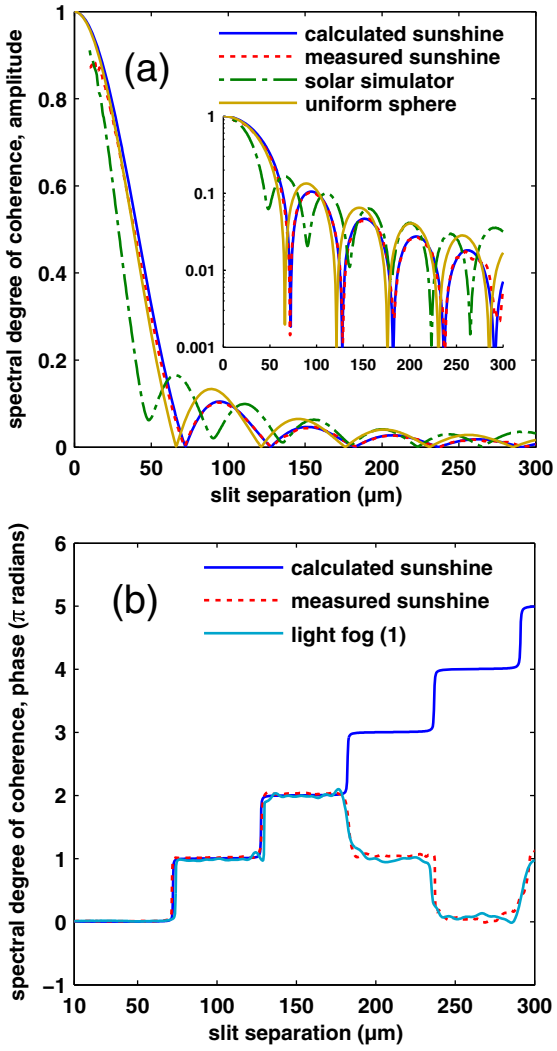

Fig. 4. Transverse spectral degree of coherence $\eta_\perp$ at 510 nm for various sources. The amplitude of $\eta_\perp$ is shown in (a) and the phase in (b). The inset in (a) shows $|\eta_\perp|$ on a logarithmic scale. The measured and calculated curves relating to sunshine in both (a) and (b) correspond to cross sections along the respective lines given in Figs. 3(a-d).

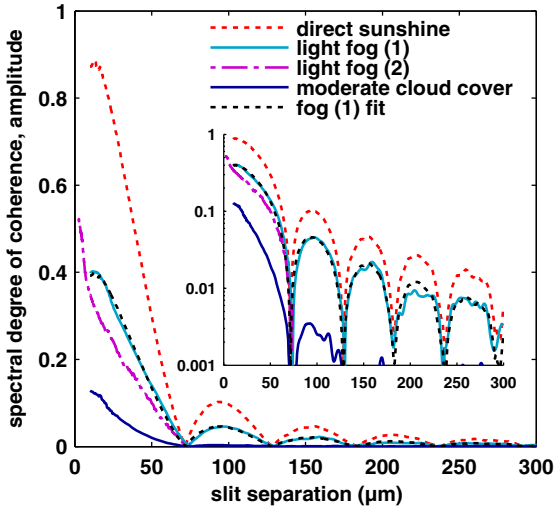

Fig. 5. Amplitude of the transverse spectral degree of coherence ($|\eta_\perp|$) at 510 nm for different weather conditions. The inset shows $|\eta_\perp|$ on a logarithmic sale. The direct sunshine case corresponds to the measured curve given in Fig. 4(a).

$r = |\vec{r_2} - \vec{r_1}|$ is the distance between points in the transverse plane. Then, ignoring the second term, Eq. (5) can be approximated by $\gamma\eta_\perp(r,\omega)$. Thus, the simple relationship between the diffuse cases and the direct function becomes clear. This approximation was used with a value $\gamma = 0.45$ in fitting the first fog case. The fit and measurement overlap significantly.

The second fog measurement was taken two minutes after the first using a slightly different system (see Appendix A). In this case, a peak-like feature related to the second term on the right-hand side of Eq. (5) becomes visible in the lowest slit separation region. This feature is significantly wider than expected by the second term. The discrepancy between the second fog measurement and the second term in Eq. (5) is due simply to the fact that the diffused light was not truly uniform. In reality, the brightness of the fog fell off for positions away from the Sun. This factor effectively narrowed the spatial distribution of the source and thus widened the part of the coherence function due to diffused light. However, even given this discrepancy, it is clear that the spatial coherence length is greatly reduced in the diffuse case as compared to the direct sunshine case. For example, using the same definition for the coherence length $L_\perp$ as before, we find for the second fog case $L_\perp = 7\lambda$ as given by Fig. 5. This length is expected by Eq. (5) to be as low as $\lambda/3$ in the extreme ($\gamma = 0$) case.

4. ARBITRARILY ORIENTED DEVICE PLANE

We proceed by describing how, in the solar disk-only case, the cross spectral density $\mathbf{W}_d(\vec{r_1},\vec{r_2},\omega)$ and spectral degree of coherence $\eta_d(\vec{r_1},\vec{r_2},\omega)$ between points in an arbitrarily oriented device plane can be given in terms of the transverse functions $\mathbf{W}_\perp(\vec{r},\omega)$ and $\eta_\perp(r,\omega)$, where $\vec{r} := \vec{r_2} - \vec{r_1}$ and $r := |\vec{r}|$. We assume a spatially incoherent, broadband source that appears circularly symmetric (but not necessarily uniform) from the origin. We define the set of rectangular coordinate axes x, y, z such that $\vec{r_1}$ and $\vec{r_2}$ lie in the x–y plane and the center of the source is located at position $\vec{r_0}$, with polar angle θ_0 and azimuthal angle ϕ_0 (see Fig. 2(b)). We assume that the source is far from the device plane such that $|\vec{r_0}|$ is much larger than r.

Now, by applying the appropriate rotation matrix to the cross-spectral density in the transverse case, we can find the cross-spectral density and spectral degree of coherence between any two points in the device plane. Let $\mathbf{M}(\theta_0,\phi_0) := \mathbf{R}_z(\phi_0)\mathbf{R}_y(\theta_0)$ where $\mathbf{R}_i(\varphi)$ is a rotation about the i axis by angle φ as given by the right-hand rule. Then, as shown explicitly in Appendix D, $\mathbf{W}_d$ and η_d can be expressed as

$$\mathbf{W}_d(\vec{r_1},\vec{r_2},\omega) \approx \mathbf{M}\mathbf{W}_\perp(\mathbf{M}^\intercal\vec{r},\omega)\mathbf{M}^\intercal \exp(-ikrp), \quad (6)$$

and

$$\eta_d(\vec{r_1},\vec{r_2},\omega) \approx \eta_\perp(r\sqrt{1-p^2},\omega)\exp(-ikrp), \quad (7)$$

where $p := \sin\theta_0\cos[\phi_0 - \vartheta]$, $\vartheta := \arctan(\vec{r}\cdot\hat{y}, \vec{r}\cdot\hat{x})$, and $\arctan(y,x)$ is the four-quadrant inverse tangent. The functions $\mathbf{W}_\perp(\vec{r},\omega)$ and $\eta_\perp(r,\omega)$ describe, respectively, the cross-spectral density and spectral degree of coherence in the transverse plane (the $\theta_0 = 0$, sunshine-only case), the latter of which is given in Fig. 3. We note that the degree of coherence between points in the transverse plane is a function of only ω and the distance r between the points; fields of this type are known as Schell-model fields [32].

Coherence functions in the general case: We now consider a device plane that is oriented obliquely to the transverse plane and illuminated by both diffuse and direct sunlight. As before, we model this situation as the combination of a disk and a half-shell (see Fig. 2(b)).

By the additive nature of the cross-spectral density for mutually-incoherent sources, and by Eqs. (3), (5), (6), and (7) we find

$$\mathbf{W}(\vec{r_1},\vec{r_2},\omega) \approx \mathbf{W}_d(\vec{r_1},\vec{r_2},\omega) + \mathbf{W}_s(\vec{r_1},\vec{r_2},\omega), \quad (8)$$

and

$$\eta(\vec{r_1},\vec{r_2},\omega) \approx \gamma\eta_\perp(r\sqrt{1-p^2},\omega)e^{-ikrp} + (1-\gamma)\frac{\sin(kr)}{kr}, \quad (9)$$

where $\mathbf{W}_s$ is the cross-spectral density in the device plane due to the uniform half-shell (explicit expressions for $\mathbf{W}_\perp$ and $\mathbf{W}_s$ are given in Appendix D).

Equations (8) and (9) are the main results of this section. They state that the cross-spectral density and spectral degree of coherence between two points in a device plane can be described by their relative distance (r), their orientation with respect to the Sun ($\theta_0, \phi_0, \vartheta$), the transverse coherence functions of direct sunshine ($\mathbf{W}_\perp$, $\eta_\perp$), the frequency (ω), and the ratio (γ) between the spectral densities in the device plane due to the Sun and a uniform cloud cover or fog. Using Eq. (9) together with our experimental results for $\eta_\perp$ we can derive the spectral degree of coherence in an arbitrarily oriented device plane.

5. IMPLICATIONS FOR THE SIMULATION OF COHERENT PHOTOVOLTAICS

In general, the electromagnetic field impinging on a device is not a plane wave but rather it fluctuates randomly in time and space. The average response of a device is thereby an ensemble average of responses to random field realizations. In simulating devices, it is not enough to consider the response under plane wave illumination; a rigorous treatment requires that they be simulated under realizations of the full field. The cross-spectral density matrix $\mathbf{W}$ is a particular measure for the statistics of these realizations. In fact, $\mathbf{W}$ as given by Eq. (8) can be used to directly generate realizations of the field [33]. Another method for generating realizations, as implied by Eq. (2), is to use a Monte Carlo simulation in which plane waves with random polarization, phase, and wave vector are coherently superposed.

For devices with a linear response, the requirements for realistic simulations become more relaxed. For some ensemble averaged observable $B(\omega)$ (absorption, external quantum efficiency, etc.), we can write [34]

$$B(\omega) = \int_{\sigma} a(\hat{u}, \omega)\chi(\hat{u}, \omega)\mathrm{d}\Omega, \tag{10}$$

where a, σ, and $\mathrm{d}\Omega$ are as before (see Problem Statement and Appendix D). χ is the generalized linear susceptibility that corresponds to the observable B and describes the response of the system to unpolarized plane waves traveling in the $\hat{u}$ direction with frequency ω. Simply, the device can be simulated under illumination by plane waves of different wave vectors and polarizations and the responses to these waves can be linearly summed with the proper weight to determine the overall response. Implementation of Eq. (10) is therefore compatible with simulation modalities that consider plane wave illumination.

It is also possible, from knowledge of the dielectric susceptibility of the scattering medium and the CSD matrix **W** of the incoming light, to determine the power spectral density distribution of light within a device. Such a calculation would involve propagating **W** into the device [13,35] and using the basic equations for scattering in random media (see Mandel and Wolf [24], Sect. 7.6) to determine the power spectrum.

6. CONCLUSIONS

We have used a double slit aperture, in which the slit separation slowly varies, to measure the transverse spectral degree of coherence of direct sunshine, sunlight diffused by clouds or fog, and light emitted by a solar simulator. The results in the direct case were compared to those expected by theory as applied to hyperspectral image data and found to agree. The results are precise enough to distinguish the true transverse spectral degree of coherence of direct sunlight from the uniform disk approximation. It was shown that, in general, the uniform disk approximation is very close to the measured function.

We have shown that the spectral degree of coherence in a plane that is arbitrarily oriented with respect to a circularly symmetric source, such as the Sun, can be derived given the transverse spectral degree of coherence. A simple model was also developed to describe the spectral degree of coherence under overcast skies. This model was shown to accurately fit the diffuse sunlight measurements in the transverse case. Further, an intuitive set of requirements was provided for the design of a solar simulator with spatial coherence properties similar to those of the Sun.

We have also described a method by which simulations of co-PVs can include the effects of partial coherence. For linear devices, an ensemble average of plane wave responses is sufficient. For non-linear devices, a rigorous treatment includes an ensemble average of the device response to random realizations of the field. We have also shown that, for devices with effective dimensions on the order of a few wavelengths or less, direct sunlight can be approximated as spatially coherent. However, this is not true for overcast skies where the coherence function falls off quickly within these dimensions. This implies that future co-PV designs should take into account the spatial coherence of sunlight, especially if the components are expected to be used under cloud cover. Additionally, co-PVs should be tested under a spatial coherence standard such that fair comparisons may be made between different devices.

APPENDIX A: MATERIALS AND METHODS

Measurement apparatus: The measurement procedure has been described previously in Ref. [21]. The measurements were performed using a stock Nikon DX-format camera sensor placed at a distance of 6.19 cm behind non-parallel slits, as shown in Fig. 1. The slit separation varies from 10 to 300 μm. 6.19 cm is sufficient to be in the far-field of the two slits together but still in the near-field of the long dimension of each slit. Consequently, diffraction can be approximated as taking place only along the direction that connects the two slits and the resulting interference pattern describes an ensemble of simultaneous Thompson-Wolf experiments [36]. The spectral degree of coherence is recovered by combining information from the interference pattern with power spectra as measured by the same device. Technically, Ref. [21] provides a method to measure the spectral degree of coherence $\mu(\vec{r_1}, \vec{r_2}, \omega)$ of a scalar field. However, under comparison with Ref. [23], it is clear that the same method measures the spectral degree of coherence $\eta(\vec{r_1}, \vec{r_2}, \omega)$ of an electromagnetic vector field.

Direct sunlight: Our measurement of direct sunlight was performed by recording only two images, one to measure the spectrum and one to measure the spectral degree of coherence. The first image, to measure the spectrum, is of an interference pattern created by illuminating the slits with sunshine reflected from a small, distant mirror. The second image is of an interference pattern created behind the aperture by direct sunshine. By using the first image to normalize the second, as described in [21], the transverse spectral degree of coherence can be measured. The measurement was made on 22 March 2013 in Zurich, Switzerland. A solar semi-diameter of 16.1 minutes, corresponding to 15 March 2013 [37], was used in the calculation of the theoretical maps. The uniform disk source calculation was also made assuming a 16.1 minute semi-diameter.

Solar simulator: The simulator consists of a xenon arc-lamp with air-mass 1.5 optical filters. Our measurement method for the solar simulator source is similar to that of the direct sunshine case. The coherence image was recorded at the device plane and the spectral image was recorded at a distance of 2 m from the source. Further, since the simulator source subtended a significant solid angle at the device plane, an extra post-processing step was required beyond those described in [21]: the spectral image was deconvolved from the coherence function image. This allowed for the retrieval of the point-spread function that, when projected along one dimension and convolved again with the spectrum image, gives the result that would be expected in the limit of very long slits and a Schell-model coherence function. The lowest spatial frequency components of the point-spread function were obscured in the particular images that were recorded. These components were recovered by extrapolation using a polynomial fit of higher frequency components.

Diffuse sunlight: For diffuse sunlight we chose a simpler measurement procedure. The transverse spectral degree of coherence corresponding to a wavelength of 510 nm was

obtained by recording only a single image. The slits were placed behind a narrow-band-pass optical filter centered at 510 nm and the equal time degree of coherence $j^{(+)}(r)$ was found using the method described in [21] and directly equated to the spectral degree of coherence via an equation first derived by Wolf [38]: $\mu(r,\omega_0) = j^{(+)}(r)$, where ω_0 is the center frequency of the optical bandpass filter. This method was used, as opposed to that used for measuring direct sunshine, because it requires only a single image to be recorded and avoids the complication of a time-varying spectral density of the source. In the second fog measurement, a 4x telescope was used to decrease the apparent size of the Sun from the point of view of the slits. The use of a telescope in this fashion is equivalent to a reduction in the slit-to-slit separation by a factor of 4. Consequently the minimum available separation was reduced from 10 to 2.5 μm.

APPENDIX B: A HALF-SHELL SOURCE

Here we consider a uniform, hemispherical, incoherent shell source, which is a simple model for cloud cover. The result given in Eq. (3) has been derived by Beran and Parrent [31] and Korotkova and Wolf [23]. The same result can also be found by applying Eq. (1) to the explicit expression for the cross-spectral density given by Blomstedt *et al.* [29] (see Eq. (D7)).

Beran and Parrent consider the cross-spectral density on the surface of a volume composed of classical isotropic radiators. They show in Eqs. (4)–(51) that, for a shell source, the spectral degree of coherence in the device plane is given by Eq. (3). Korotkova and Wolf apply Eq. (1) to the cross-spectral density matrix given by Mehta and Wolf [39]. While the cross-spectral density matrix given by Mehta and Wolf [39] differs from that given by Blomstedt *et al.* [29], they both return the same expression for the spectral degree of coherence as defined by Eq. (1).

APPENDIX C: A COMBINED DISK-SHELL SOURCE

Here we discuss the derivation of Eq. (4). Returning to Eq. (2), we consider a spectral density distribution given by $a(\hat{u},\omega) \coloneqq a_d(\hat{u},\omega) + a_s(\hat{u},\omega)$, where $a_d(\hat{u},\omega)$ is the spectral density distribution of the disk and $a_s(\hat{u},\omega)$ is the spectral density distribution of the shell, as shown in Fig. 2(b), and we have assumed very distant sources. Then $\mathbf{W}(\vec{r_1},\vec{r_2},\omega) = \mathbf{W}_d(\vec{r_1},\vec{r_2},\omega) + \mathbf{W}_s(\vec{r_1},\vec{r_2},\omega)$, where $\mathbf{W}_d$ and $\mathbf{W}_s$ are the cross-spectral densities that would be found for the disk and shell alone, respectively. Let $s_d(\omega) \coloneqq \mathrm{Tr}[\mathbf{W}_d(\vec{r_1},\vec{r_1},\omega)] = \mathrm{Tr}[\mathbf{W}_d(\vec{r_2},\vec{r_2},\omega)]$ and $s_s(\omega) \coloneqq \mathrm{Tr}[\mathbf{W}_s(\vec{r_1},\vec{r_1},\omega)] = \mathrm{Tr}[\mathbf{W}_s(\vec{r_2},\vec{r_2},\omega)]$, where s_d and s_s represent the spectral densities at $\vec{r_1}$ and $\vec{r_2}$ (the spectral density at both points is the same under these conditions) due to the disk and shell, respectively. Then, by Eq. (1), $\eta_d(\vec{r_1},\vec{r_2},\omega) = \mathrm{Tr}[\mathbf{W}_d(\vec{r_1},\vec{r_2},\omega)]/s_d(\omega)$ and $\eta_s(\vec{r_1},\vec{r_2},\omega) = \mathrm{Tr}[\mathbf{W}_s(\vec{r_1},\vec{r_2},\omega)]/s_s(\omega)$. Since $\mathrm{Tr}[\mathbf{A}+\mathbf{B}] = \mathrm{Tr}[\mathbf{A}] + \mathrm{Tr}[\mathbf{B}]$, this leads directly to Eq. (4).

APPENDIX D: THE CROSS-SPECTRAL DENSITY OF DIRECT AND DIFFUSE SUNLIGHT

Here we derive expressions for the cross-spectral density and spectral degree of coherence of direct and diffuse sunlight. For the solar disk centered on the z axis, $a(\hat{u},\omega) = \Theta(\theta_d - \theta)a_\theta(\theta,\omega)$ for some function $a_\theta(\theta,\omega)$ where $\Theta(x)$ is the unit-step function and θ_d is the angular semi-diameter of the source. Under the uniform disk approximation, $a_\theta(\theta,\omega) = a_0(\omega)$ where $a_0(\omega)$ represents a power spectral density of the disk per unit solid angle. In the more accurate limb-darkened case, a good approximation is given by $a_\theta(\theta,\omega) = a_0(\omega)\sum_{n=0}^{5} A_n(\omega)\psi(\theta)^n$, where

$$\psi(\theta) \coloneqq \frac{\sqrt{\sin^2\theta_d - \sin^2\theta}}{\sin\theta_d} \tag{D1}$$

and each $A_n(\omega)$ represents a coefficient that can be 2-D interpolated from solar limb-darkening data (see Ref. [22], Table 1). In either case Eq. (2) gives

$$\mathbf{W}(\vec{r_1},\vec{r_2},\omega) \approx \exp(-ik\hat{z}^\intercal\vec{r}) \int_0^{\theta_d}\int_0^{2\pi} a_\theta(\theta,\omega)(\mathbf{U}_3 - \hat{u}\hat{u}^\intercal) \times \exp(ik\vec{\sigma}\cdot\vec{\rho}) \sin\theta \mathrm{d}\phi\mathrm{d}\theta, \tag{D2}$$

where $\vec{\sigma} \coloneqq -\sin\theta\cos\phi\hat{x} - \sin\theta\sin\phi\hat{y}$, $\vec{\rho} \coloneqq \mathbf{U}_2\vec{r}$, $\mathbf{U}_2 \coloneqq \hat{x}\hat{x}^\intercal + \hat{y}\hat{y}^\intercal$, and we have used the small angle approximation $\cos\theta \approx 1$. The approximation is justified by the fact that the angular semi-diameter θ_d of the Sun is always less than 16.5 arcminutes ≈0.0048 radians [37]. In the transverse plane, $\vec{r_1}$ and $\vec{r_2}$ have no z component which implies a definition for the transverse cross-spectral density

$$\mathbf{W}_\perp(\vec{r},\omega) \coloneqq \int_0^{\theta_d}\int_0^{2\pi} a_\theta(\theta,\omega)(\mathbf{U}_3 - \hat{u}\hat{u}^\intercal) \times \exp(ik\vec{\sigma}\cdot\vec{\rho}) \sin\theta \mathrm{d}\phi\mathrm{d}\theta, \tag{D3}$$

which further implies

$$\mathbf{W}(\vec{r_1},\vec{r_2},\omega) \approx \exp(-ik\hat{z}^\intercal\vec{r})\mathbf{W}_\perp(\vec{r},\omega). \tag{D4}$$

$\mathbf{W}_\perp$ itself implies a definition for the transverse spectral degree of coherence $\eta_\perp(\vec{r},\omega) \coloneqq \mathrm{Tr}[\mathbf{W}_\perp(\vec{r},\omega)]/\mathrm{Tr}[\mathbf{W}_\perp(\vec{0},\omega)]$.

The general case of a solar disk centered at polar angle θ_0 and azimuthal angle ϕ_0 (see Fig. 2(b)) can be found using the rotation matrix

$$\mathbf{M}(\theta,\phi) \coloneqq \mathbf{R}_z(\phi)\mathbf{R}_y(\theta) = \begin{pmatrix} \cos\phi\cos\theta & -\sin\phi & \cos\phi\sin\theta \\ \cos\theta\sin\phi & \cos\phi & \sin\phi\sin\theta \\ -\sin\theta & 0 & \cos\theta \end{pmatrix}. \tag{D5}$$

The rotation of a vector field $\vec{F}(\vec{r})$ using a rotation matrix $\mathbf{R}$ is given by $\mathbf{R}\vec{F}(\mathbf{R}^\intercal\vec{r})$. Since $\mathbf{W}(\vec{r_1},\vec{r_2},\omega) = \langle\vec{E}^*(\vec{r_1},\omega)\vec{E}^\intercal(\vec{r_2},\omega)\rangle$, the general solar disk case $\mathbf{W}_d$ is found by applying $\mathbf{M}(\theta_0,\phi_0)$ to Eq. (D4), after noting that the

z component of both $\vec{r_1}$ and $\vec{r_2}$ is zero in the device plane, which gives Eq. (6).

An explicit expression for $\mathbf{W}_\perp$ can be found under the uniform disk and small angle approximations by straightforward application of the method given by Blomstedt *et al.* [29], Appendix A, and is given to second order in θ_d by

$$\mathbf{W}_\perp(\vec{r},\omega) \approx 2\pi a_d(\omega)\left\{\left[\theta_d\frac{J_1(\alpha)}{\beta} - \theta_d^2\frac{J_2(\alpha)}{\beta^2}\right]\mathbf{U}_2 + 2\theta_d^2\frac{J_2(\alpha)}{\beta^2}\hat{z}\hat{z}^\intercal + i\theta_d^2\frac{J_2(\alpha)}{\beta}[\hat{\rho}\hat{z}^\intercal + \hat{z}\hat{\rho}^\intercal]\right\}, \quad \textbf{(D6)}$$

where $\alpha := k\rho\theta_d$, $\beta := k\rho$, $\rho := |\vec{\rho}|$, $\hat{\rho} := \vec{\rho}/\rho$, each J_i is a Bessel function of order i, and a_d is the appropriate power spectral density for direct sunlight (see Fig. 2(b)). From the above equation it is clear that $\eta_\perp(\vec{r},\omega)$ is a function of ρ alone, that is, $\eta_\perp(\vec{r},\omega)$ can be written as $\eta_\perp(\rho,\omega)$; this can be shown to hold in general for any circularly symmetric source and the function $\eta_\perp(\rho,\omega)$ is given for sunshine (denoted $\eta_\perp(r,\omega)$) in Fig. 3. Finally, combining the facts that $r = \rho = |\mathbf{U}_2\vec{r}|$ in the transverse plane, $|\mathbf{U}_2\vec{r}| \to |\mathbf{U}_2\mathbf{M}^\intercal\vec{r}|$ under rotation, and that the matrix trace is invariant under similarity transformations, Eq. (7) follows immediately from Eq. (6).

For reference, $\mathbf{W}_s$ is given by Blomstedt *et al.* [29], Eq. (D4), as

$$\mathbf{W}_s(\vec{r_1},\vec{r_2},\omega) = 2\pi a_s(\omega)\left\{\left[j_0(\beta) - \frac{j_1(\beta)}{\beta}\right]\mathbf{U}_3 + j_2(\beta)\hat{\rho}\hat{\rho}^\intercal + i\frac{J_2(\beta)}{\beta}[\hat{\rho}\hat{z}^\intercal + \hat{z}\hat{\rho}^\intercal]\right\}, \quad \textbf{(D7)}$$

where each j_i is a spherical Bessel function of order i and a_s is the appropriate power spectral density for diffuse sunlight. The equation above has a sign change in front of the imaginary term relative to the expression given by Blomstedt *et al.* due to a difference in definitions of coordinate axes.

APPENDIX E: THE CROSS-SPECTRAL DENSITY MATRIX OF PARTIALLY POLARIZED SKYLIGHT

Here we discuss the CSD matrix $\mathbf{W}_y$ due to partially polarized skylight alone. We begin by noting that skylight is relatively minor compared to direct sunlight in contributing to the total power that strikes the surface of the Earth, making up about 10% of the total under the AM 1.5 standard [40]. Although polarized, skylight is expected to be angularly uncorrelated as it originates from a single scattering of sunlight [26]. This allows $\mathbf{W}_y$ to be decomposed, with knowledge of the spatial distribution of the degree and direction of polarization (see Bohren [26], section 3), into two separate matrices, $\mathbf{W}_p$ and $\mathbf{W}_u$, which correspond to the CSDs of completely polarized and unpolarized skylight, respectively. These matrices would be added to the right-hand side of Eq. (8), and $\mathbf{W}_s$ removed, in order to take pure skylight into account. The use of Eq. (2) is sufficient for calculating $\mathbf{W}_u$ but not $\mathbf{W}_p$. To calculate $\mathbf{W}_p$ one can use the more general expression given by Blomstedt *et al.* [29], Eq. (4).

FUNDING INFORMATION

Swiss National Science Foundation (SNSF) (200021_149433).

ACKNOWLEDGMENT

We thank Z. J. Lapin, P. Bharadwaj, and M. Kasperczyk for fruitful discussions and M. Parzefall for help in creating figures of this paper.

REFERENCES AND NOTES

1. M. A. Green, K. Emery, Y. Hishikawa, W. Warta, and E. D. Dunlop, "Solar cell efficiency tables (version 43)," Prog. Photovoltaics **22**, 1–9 (2014).
2. A. Polman and H. A. Atwater, "Photonic design principles for ultra-high-efficiency photovoltaics," Nat. Mater. **11**, 174–177 (2012).
3. E. Garnett and P. Yang, "Light trapping in silicon nanowire solar cells," Nano Lett. **10**, 1082–1087 (2010).
4. V. E. Ferry, M. A. Verschuuren, M. C. v. Lare, R. E. I. Schropp, H. A. Atwater, and A. Polman, "Optimized spatial correlations for broadband light trapping nanopatterns in high efficiency ultrathin film a-Si:H solar cells," Nano Lett. **11**, 4239–4245 (2011).
5. C. Battaglia, C.-M. Hsu, K. Söderström, J. Escarré, F.-J. Haug, M. Charrière, M. Boccard, M. Despeisse, D. T. L. Alexander, M. Cantoni, Y. Cui, and C. Ballif, "Light trapping in solar cells: Can periodic beat random?" ACS Nano **6**, 2790–2797 (2012).
6. R. A. Pala, J. S. Liu, E. S. Barnard, D. Askarov, E. C. Garnett, S. Fan, and M. L. Brongersma, "Optimization of non-periodic plasmonic light-trapping layers for thin-film solar cells," Nat. Commun. **4**, 2095 (2013).
7. M. van Lare, F. Lenzmann, and A. Polman, "Dielectric back scattering patterns for light trapping in thin-film Si solar cells," Opt. Express **21**, 20738–20746 (2013).
8. Y. Kuang, M. D. Vece, J. K. Rath, L. van Dijk, and R. E. I. Schropp, "Elongated nanostructures for radial junction solar cells," Rep. Prog. Phys. **76**, 106502 (2013).
9. M. L. Brongersma, Y. Cui, and S. Fan, "Light management for photovoltaics using high-index nanostructures," Nat. Mater. **13**, 451–460 (2014).
10. T. Sun, C. Fei Guo, F. Cao, E. Metin Akinoglu, Y. Wang, M. Giersig, Z. Ren, and K. Kempa, "A broadband solar absorber with 12 nm thick ultrathin a-Si layer by using random metallic nanomeshes," Appl. Phys. Lett. **104**, 251119 (2014).
11. S. Pattnaik, N. Chakravarty, R. Biswas, V. Dalal, and D. Slafer, "Nano-photonic and nano-plasmonic enhancements in thin film silicon solar cells," Sol. Energ. Mat. Sol. C. **129**, 115–123 (2014).
12. S. Morawiec, M. J. Mendes, S. A. Filonovich, T. Mateus, S. Mirabella, H. Águas, I. Ferreira, F. Simone, E. Fortunato, R. Martins, F. Priolo, and I. Crupi, "Broadband photocurrent enhancement in a-Si:H solar cells with plasmonic back reflectors," Opt. Express **22**, A1059–A1070 (2014).
13. The statistical correlations of light obey precise propagation laws as given in Ref. (24) p. 182–183. Specifically, the ensemble average behavior of an optical system depends on the cross-spectral density of incident light, which is a measure for the spectral dependence of the spatial coherence.
14. G. Moddel, "Will rectenna solar cells be practical?" in *Rectenna Solar Cells*, G. Moddel and S. Grover, eds. (Springer, 2013), pp. 3–24.
15. R. E. Collin and F. J. Zucker, *Antenna Theory Part 1* (McGraw-Hill, 1969).
16. M. E. Verdet, *Leçons d'Optique Physique*, vol. **1** (L'Imprimerie Impériale, 1869).
17. G. S. Agarwal, G. Gbur, and E. Wolf, "Coherence properties of sunlight," Opt. Lett. **29**, 459–461 (2004).

18. A. T. Friberg and E. Wolf, "Relationships between the complex degrees of coherence in the space–time and in the space–frequency domains," Opt. Lett. **20**, 623–625 (1995).
19. H. Mashaal, A. Goldstein, D. Feuermann, and J. M. Gordon, "First direct measurement of the spatial coherence of sunlight," Opt. Lett. **37**, 3516–3518 (2012).
20. H. Mashaal and J. M. Gordon, "Fundamental bounds for antenna harvesting of sunlight," Opt. Lett. **36**, 900–902 (2011).
21. S. Divitt, Z. J. Lapin, and L. Novotny, "Measuring coherence functions using non-parallel double slits," Opt. Express **22**, 8277–8290 (2014).
22. H. Neckel and D. Labs, "Solar limb darkening 1986–1990 (λλ303 to 1099 nm)," Sol. Phys. **153**, 91–114 (1994).
23. O. Korotkova and E. Wolf, "Spectral degree of coherence of a random three-dimensional electromagnetic field," J. Opt. Soc. Am. A **21**, 2382–2385 (2004).
24. L. Mandel and E. Wolf, *Optical Coherence and Quantum Optics* (Cambridge University Press, 1995).
25. T. Setälä, J. Tervo, and A. T. Friberg, "Complete electromagnetic coherence in the space-frequency domain," Opt. Lett. **29**, 328–330 (2004).
26. C. F. Bohren, "Atmospheric optics," in *The Optics Encyclopedia* (Wiley-VCH Verlag GmbH and Co. KGaA, 2007).
27. M. Born and E. Wolf, *Principles of Optics*, 7th ed. (Cambridge University, 1999).
28. T. Setälä, M. Kaivola, and A. T. Friberg, "Spatial correlations and degree of polarization in homogeneous electromagnetic fields," Opt. Lett. **28**, 1069–1071 (2003).
29. K. Blomstedt, T. Setälä, J. Tervo, J. Turunen, and A. T. Friberg, "Partial polarization and electromagnetic spatial coherence of blackbody radiation emanating from an aperture," Phys. Rev. A **88**, 013824 (2013).
30. L. Novotny and B. Hecht, *Principles of Nano-Optics*, 2nd ed. (Cambridge University, 2012).
31. M. Beran and G. Parrent, Jr., *Theory of Partial Coherence* (The Society of Photo-optical Instrumentation Engineers, 1974).
32. E. Wolf, *Introduction to the Theory of Coherence and Polarization of Light* (Cambridge University, 2007).
33. R. Popescu, G. Deodatis, and J. Prevost, "Simulation of homogeneous nonGaussian stochastic vector fields," Probabilist. Eng. Mech. **13**, 1–13 (1998).
34. J. Jensen and A. R. Mackintosh, *Rare Earth Magnetism: Structures and Excitations* (Clarendon, 1991).
35. M. Lahiri and E. Wolf, "Propagation of electromagnetic beams of any state of spatial coherence and polarization through multilayered stratified media," J. Opt. Soc. Am. A **30**, 2547–2555 (2013).
36. B. J. Thompson and E. Wolf, "Two-beam interference with partially coherent light," J. Opt. Soc. Am. **47**, 895 (1957).
37. U. S. N. A. Office, *Astronomical Almanac for the Year 2013* (United States Naval Observatory/Nautical Almanac Office, 2012).
38. E. Wolf, "Young's interference fringes with narrow-band light," Opt. Lett. **8**, 250–252 (1983).
39. C. L. Mehta and E. Wolf, "Coherence properties of blackbody radiation. III. Cross-spectral tensors," Phys. Rev. **161**, 1328–1334 (1967).
40. ASTM G173-03(2012), "Standard tables for reference solar spectral irradiances: Direct normal and hemispherical on 37° tilted surface," (2012). ASTM International.